

## COMPARING THE EVOLUTION OF THE GALAXY DISK SIZES WITH COLD DARK MATTER MODELS: THE HUBBLE DEEP FIELD

E. GIALLONGO,<sup>1</sup> N. MENCI,<sup>1</sup> F. POLI,<sup>1</sup> S. D'ODORICO,<sup>2</sup> AND A. FONTANA<sup>1</sup>

*Received 1999 November 26; accepted 1999 December 22; published 2000 January 31*

### ABSTRACT

The intrinsic sizes of the field galaxies with  $I \leq 26$  in the Hubble and ESO New Technology Telescope (NTT) Deep Fields are shown as a function of their redshifts and absolute magnitudes using photometric redshifts derived from the multicolor catalogs and are compared with the cold dark matter (CDM) predictions. Extending to the lower luminosities and to the higher  $z$  that our previous analysis performed on the NTT field alone, we find the distribution of the galaxy disk sizes at different cosmic epochs is within the range predicted by typical CDM models. However, the observed size distribution of faint ( $M_B > -19$ ) galaxies is skewed with respect to the CDM predictions, and an excess of small-size disks ( $R_d < 2$  kpc) is already present at  $z \sim 0.5$ . The excess persists up to  $z \sim 3$  and involves brighter galaxies. Such an excess may be reduced if luminosity-dependent effects, like starburst activity in interacting galaxies, are included in the physical mechanisms governing the star formation history in CDM models.

*Subject headings:* galaxies: evolution — galaxies: formation — galaxies: fundamental parameters

### 1. INTRODUCTION

Our understanding of galaxy formation has recently undergone some appreciable progress. Observationally, this is due to the new photometric and spectroscopic information on deep galaxy fields. Corresponding theoretical progress has also been achieved with the development of semianalytical approaches, including the gas cooling and star formation processes, to the well-developed hierarchical clustering theories for dark matter (DM) halos; this allows us to relate the galaxy DM circular velocities to observable, luminous properties. In this context, the Tully-Fisher (TF) relation represents a typical test for the present theoretical models, as it relates the total luminosity of a disk galaxy to its halo circular velocity.

However, from an observational point of view, the measure of circular velocity is limited to bright nearby spiral galaxies and a few very bright galaxies at intermediate redshifts (e.g., Vogt et al. 1997). Extending the TF relation to fainter/distant spiral galaxies is essential for testing the evolution in the ( $L$ ,  $z$ )-plane of the  $M/L$  ratio predicted by cold dark matter (CDM) theories.

An alternative statistical approach connecting the luminous and dynamical properties of galaxy disks is based on the size-luminosity relation, once a specific model is assumed to connect size to circular velocity. This has the advantage of exploring the dynamical evolution over a wide range of luminosities and redshifts.

In a previous paper (Poli et al. 1999, hereafter Paper I), we applied this novel approach to the ESO New Technology Telescope (NTT) Deep Field (Arnouts et al. 1999) in order to derive the morphological information for the galaxies in the field down to  $I = 25$  after appropriate seeing deconvolution. The derived intrinsic angular sizes were then converted into physical sizes by adopting photometric redshifts for each galaxy in the catalog (Fontana et al. 2000). The distribution of sizes in the ( $L$ ,  $z$ )-plane was compared with the predictions of CDM semianalytic models of galaxy formation (e.g., Cole et al. 1994; Baugh et

al. 1998), complemented with the specific size-velocity relation worked out by Mo, Mao, & White (1998) for rotationally supported disks. This analysis shows an excess of small-size low-luminosity galaxies at small, intermediate redshifts. However, no assessment of this excess at higher redshifts was allowed under the sample magnitude limit. Here we want to extend the study to higher  $z$  and lower  $L$  using the available data in the Hubble Deep Field North where morphological information on the faint galaxy sample is available in the literature (Abraham et al. 1996; Odewahn et al. 1996; Driver et al. 1998; Marleau & Simard 1998). This will allow us to assess whether the excess observed at intermediate redshifts is an evolutionary effect or whether it is present at higher  $z$  also, indicating the presence of remarkable physical processes not included in the standard CDM models.

### 2. THE GALAXY CATALOG

The morphological information on the galaxies in the Hubble Deep Field North (HDF-N) was obtained using the galaxy catalog by Marleau & Simard (1998) in which the structural parameter values were derived from the intensity profile fitting. Exponential profiles were assumed for the disk component, and a final characteristic disk radius in arcseconds was computed for all the galaxies up to  $I \approx 26$ . The HDF-N galaxy catalog has been joined with the NTT Deep Field catalog used in Paper I, limited to  $I \approx 25$ .

To each galaxy in the joined catalog, a photometric redshift estimate was assigned with the same best-fitting procedure applied in Paper I and in Giallongo et al. (1998). This was obtained through a comparison of the observed colors with those predicted by spectral synthesis models (Bruzual & Charlot 1993), including UV absorption by the intergalactic medium and dust reddening. The aperture magnitudes that were used to estimate the galaxy colors and the  $I$  total magnitude for each galaxy were extracted from the catalog by Fernandez-Soto, Lanzetta, & Yahil (1999). The catalog of the photometric redshifts is presented in Fontana et al. (2000). The resulting typical redshift accuracy is  $\Delta z \approx 0.06$  up to  $z \sim 1.5$  and  $\Delta z \sim 0.3$  at larger redshifts. As derived in other fields of similar depth, the

<sup>1</sup> Osservatorio Astronomico di Roma, Via Frascati 33, Monteporzio Catone, Roma, I-00040, Italy.

<sup>2</sup> European Southern Observatory, Karl-Schwarzschild-Strasse 2, Garching bei München, D-85748, Germany.

bulk of the galaxies is concentrated at intermediate redshifts  $z \sim 0.5-1$  with a tail in the distribution up to  $z \sim 6$ .

In order to verify the effects of the background noise on the measured sizes of the faint galaxies in the HDF, we have performed a set of simulations specifically designed to reproduce the typical conditions of real data. The same test has been performed in Paper I for the galaxies in the NTT Deep Field.

The intensity profiles were reproduced as in the observed HDF images by assuming the same pixel sampling. Assuming an intrinsic exponential profile, a series of synthetic images were constructed using different half-light radii ranging from  $r_{\text{hl}} = 0''.1$  to  $r_{\text{hl}} = 0''.9$  with a step of  $0''.1$ . An average of 25 random objects were computed for each radius, assuming a total magnitude of  $I \sim 26$ , which is the limiting magnitude of the morphological galaxy sample. The background-subtracted image of a bright star was selected in the field to reproduce the instrumental point-spread function. Its normalized profile was then convolved with the synthetic images of the disk galaxies. The convolved two-dimensional profiles were randomly inserted in regions of the HDF far from the very bright objects in order to reproduce the observed HDF galaxies with the appropriate pixel size and noise levels. Finally, the multi-Gaussian deconvolution technique was applied to the synthetic data as in Paper I.

We first notice that there is no selection bias against galaxies with large size ( $r_{\text{hl}} \sim 1''$ ) and low surface brightness down to  $I \approx 26$  since all the synthetic objects were detected. The results are shown in Figure 1, where the error bars represent the dispersion around the mean that is due to noise in the background subtraction. A good match between the intrinsic and measured half-light radii was obtained up to  $r_{\text{hl}} \sim 0''.7$ . For larger values, a slight underestimate in the measured values appears at the sample-limiting magnitude. In any case, it can be seen that, even for the faint galaxies with  $I \sim 26$ , the overall correlation between intrinsic and measured half-light radii is preserved in such a way that an intrinsically large, faint object, e.g., with  $r_{\text{hl}} \sim 0''.7$ , cannot be detected as a small-sized one, e.g., with  $r_{\text{hl}} \sim 0''.1$ . The simulation shows that the fraction of small-size galaxies present in the HDF morphological catalog is real and is not due to intrinsically larger objects that have been shrunk by noise effects.

### 3. DISTRIBUTION OF GALAXY SIZES IN LUMINOSITY AND REDSHIFT: A COMPARISON WITH CDM MODELS

We have computed the disk linear size  $R_d$  and the absolute blue magnitude for each galaxy in the catalog using the color-estimated redshifts as discussed in the previous section. In Figure 2, we plot the distribution of the observed sizes for the HDF galaxies as a function of luminosity in four different redshift intervals. The filled circles represent HDF spiral galaxies with a bulge-to-total ratio in the range  $0.05 < B/T < 0.75$ , while the asterisks represent galaxies with  $B/T < 0.05$ , most of which are of irregular morphology (Marleau & Simard 1998). HDF galaxies with  $B/T > 0.75$  are excluded since they are bulge-dominated systems. The NTT Deep Field galaxies of Paper I are also shown as open squares.

In the shaded area of Figure 2, we also show the prediction of our rendition of the standard semianalytical CDM models. This relates the luminous properties of galaxies to their circular velocity, including the hierarchical merging of DM halos, the merging of galaxies inside the halos, the gas cooling, the star

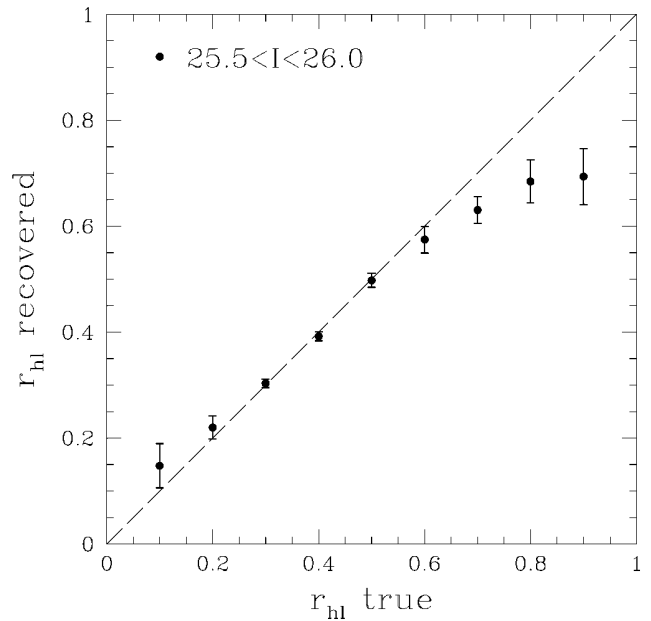


FIG. 1.—Deconvolved half-light radii as a function of true values in simulated data of the HDF. Error bars are  $1\sigma$  confidence intervals.

formation, and the supernovae feedback associated with the galaxies. Finally, the circular velocity of the halos is connected to the disk scale length using the Mo et al. (1998) model; the latter correlation depends on the dimensionless angular momentum  $\lambda$  whose lognormal distribution  $p(\lambda)$  is given in Mo et al. (1998). The shaded area in Figure 2 corresponds to that allowed for  $0.025 < \lambda < 0.1$ , the values corresponding to the 10% and 90% points of  $p(\lambda)$ . The solid line corresponds to  $\lambda = 0.05$ , the 50% point of  $p(\lambda)$ . The full  $p(\lambda)$  distribution is taken into account in the differential size distribution of galaxies with  $I < 26$  (normalized to the total number), which is shown in Figure 3 for different redshift bins. A tilted CDM power spectrum of perturbations with  $n = 0.8$  in an  $\Omega = 1$  universe with  $H_0 = 50 \text{ km s}^{-1} \text{ Mpc}^{-1}$  has been used.

The full details of our semianalytic model are given in Appendix A of Paper I, together with the adopted set of star formation and feedback parameters. The latter set was chosen so as to optimize the matching to the local  $I$ -band TF relation for bright galaxies and the  $B$ -band galaxy luminosity function. Note that, since the disk velocity is  $\sim 20\%$  higher than that of the DM, a small offset ( $\sim 0.5$  mag) between the predicted and the observed TF relation is present (see Fig. 9 of Paper I).

Figure 2 shows that at  $z < 1$  and for faint magnitudes ( $M_B > -19$ ), the observed sizes tend to occupy preferentially the small-size region below the 50% locus of the angular momentum distribution. Correspondingly, Figure 3 shows the excess of small-size ( $R_d < 2 \text{ kpc}$ ) galaxies with respect to the CDM predictions. Indeed, for  $M_B > -19$ , the predicted average disk size is  $2.1 \text{ kpc}$ , while the observed one is  $1.4 \text{ kpc}$ . These results are similar to those presented in Paper I, although extended down to  $M_B < -16$  and with larger statistics.

The excess becomes less evident at brighter magnitudes, in agreement with recent studies (Lilly et al. 1998; Simard et al. 1999) that indicate little evolution in the morphological properties of bright spiral galaxies in the Canada France Redshift Survey sample up to  $z \sim 1$ . At  $z \geq 1$ , the larger statistics avail-

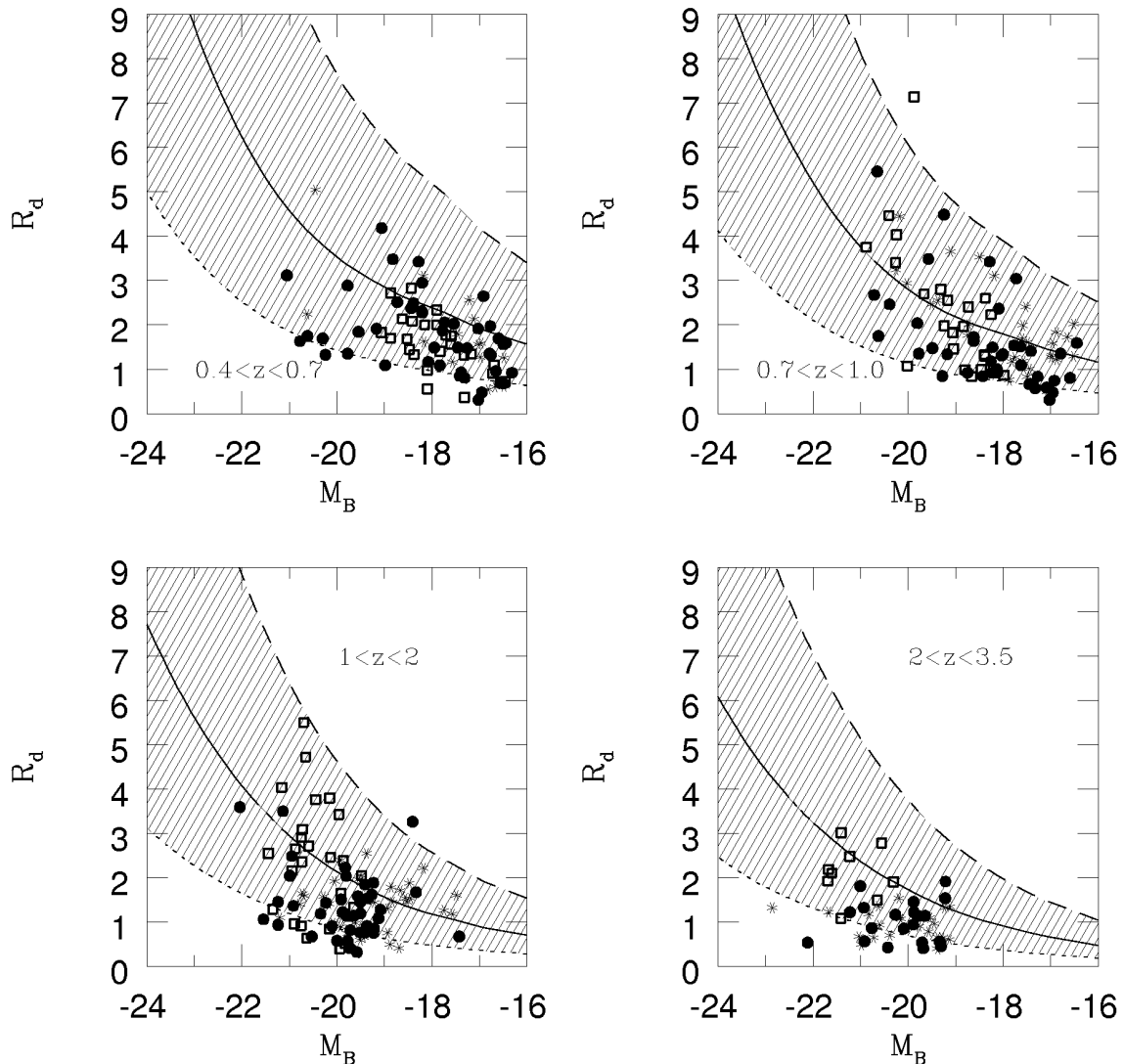


FIG. 2.—Distribution of galaxies in the luminosity-size plane in four redshift intervals. The disk radii are in kiloparsecs. The open squares are NTT Deep Field galaxies; the filled circles are HDF spiral galaxies with  $0.05 < B/T < 0.75$ ; the asterisks are galaxies with  $B/T < 0.05$ , most of which are of irregular morphology. The shaded region represents the region allowed by the model. The upper and lower lines correspond to the 90% and 10% points of the angular momentum distribution. The solid line corresponds to the 50% point of the same distribution (see the text for details).

able with the present sample (with respect to that used in Paper I) show that the excess persists and involves brighter galaxies ( $M_B \gtrsim -20$ ) with an observed average  $R_d \approx 1.3$  kpc with respect to the predicted  $R_d \approx 1.9$  kpc. In addition, the excess appears for all the galaxies in the sample regardless of their morphological classification and therefore does not depend on the selection procedure adopted for the spiral sample. Furthermore, the above excesses cannot be due to the offset (only  $\sim 0.5$  mag) between the observed and the theoretical TF relation, as confirmed by the good agreement of the  $R_d$ - $M_B$  relation at the bright end.

In summary, Figures 2 and 3 indicate that small-size galaxies appear smaller and/or brighter than predicted by CDM at all  $z$  (indeed, even more at high  $z$ ). Within the framework of the adopted standard scenario of disk formation, which assumes the conservation of the specific baryonic angular momentum (Mo et al. 1998), a viable solution consists in introducing a brightening of small-size galaxies. In particular, we note that

shifting the predicted curves toward higher luminosities results in a better fit to the data. At  $z \lesssim 1$ , the best-fitting shift is  $\sim 1$  mag, while at larger  $z$ , the best-fitting shift is  $\sim 1.5$  mag (Fig. 2).

#### 4. CONCLUSIONS AND DISCUSSION

The present analysis, performed on a larger and deeper sample, confirms our previous findings at  $z \lesssim 1$  (Paper I), where an excess of faint ( $M_B > -19$ ), small-size ( $R_d < 2$  kpc) galaxies with respect to the CDM predictions was found. The results presented here show that the excess persists even at higher redshifts ( $1 < z < 3.5$ ) and for brighter galaxies ( $M_B > -20$ ). Several processes may be responsible for the above excess (see Paper I), like the nonconservation of the gas angular momentum during the collapse in the Mo et al. (1998) model. Alternatively, within the Mo et al. framework for disk formation, a

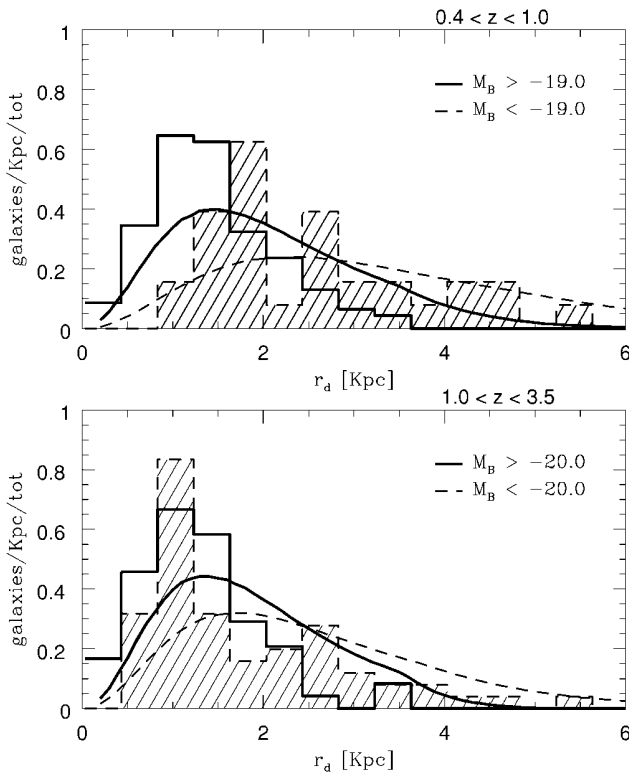


FIG. 3.—Size distribution of the low- and high-luminosity spiral galaxies in the HDF and NTT Deep Field shown in Fig. 2. The corresponding curves are the distributions predicted by the CDM model. An excess of small-size galaxies with respect to the CDM predictions is apparent at  $R_d = 1$  kpc.

possible explanation can be sought in luminosity-dependent effects related to the physical mechanisms involved in star formation activity already at high  $z$ . Indeed, a shift of the shaded region (the CDM prediction) by  $\sim 1$  mag at  $z < 1$  and by

$1.5$  mag at  $z > 1.5$  is sufficient to reconcile the CDM predictions with the observations.

Such shifts could be due to the starburst brightening of the numerous small-size galaxies subject to close encounters/interactions. This brightening would have the advantage of explaining at the same time the flat shape of the global cosmological star formation rate  $\dot{M}_*$  observed at  $z > 1.5$  in deep surveys (Steidel et al. 1999; Fontana et al. 1999); this rate is a factor of  $\sim 5$ – $10$  higher than predicted by CDM. Since the star formation rate (SFR) is proportional to the UV– $B$  luminosity, a brightening of the predicted luminosities in small-size galaxies by  $\sim 1$ – $2$  mag is needed in both cases. The interaction rate needed to reconcile the CDM evolutionary scenario with the various observables can be derived by the following simple considerations. The SFR in a galaxy halo from a cool gas of mass  $M_{\text{cool}}$  can be written as  $\dot{M}_* \approx f_{\text{gas}} M_{\text{cool}} / \tau_i + (1 - f_{\text{gas}}) M_{\text{cool}} / \tau_*$ , where  $f_{\text{gas}}$  is the fraction of gas converted into stars because of interactions,  $\tau_i$  is the timescale for interactions, and  $\tau_*$  is the quiescent star formation timescale. While only the latter term is usually included in the CDM models, we note that for  $f_{\text{gas}} \sim 0.1$ , a  $\tau_i$  shorter than  $\tau_*$  by about a factor of 100 would be implied in order to obtain a SFR consistent with the high- $z$  data; for the population of small galaxies (dominating at high  $z$ ) with a circular velocity  $v_c \lesssim 100$  km s $^{-1}$  (corresponding to  $\tau_* \approx 5$  Gyr; see Cole et al. 1994), this would imply a  $\tau_i \approx 0.1$  Gyr, which is in fact close to the dynamical timescale of these systems at  $z \sim 2$ . Note that for larger ( $v_c > 200$  km s $^{-1}$ ) disk galaxies,  $\tau_* \sim v_c^{-1.5}$  becomes smaller while  $\tau_i \sim 1/N_g$  remains large because of the small number density  $N_g$  (Cavaliere & Vittorini 2000), so that the quiescent star formation mode prevails for these systems; in addition, since  $N_g \sim (1+z)^3$  for all the galaxies, the interaction timescale  $\tau_i$  becomes ineffective at small  $z$ . Detailed implementation of the interaction-driven star formation mode in semianalytical models will soon provide a more quantitative test for the importance of this physical mechanism in determining the galaxy properties at high  $z$ .

#### REFERENCES

- Abraham, R. G., Tanvir, N. R., Santiago, B., Ellis, R. S., Glazebrook, K., & van den Berg, S. 1996, *MNRAS*, 279, L47  
 Arnouts, S., D’Odorico, S., Cristiani, S., Zaggia, S., Fontana, A., & Giallongo, E. 1999, *A&A*, 341, 641  
 Baugh, C. M., Cole, S., Frenk, C. S., & Lacey, C. G. 1998, *ApJ*, 498, 504  
 Bruzual A., G., & Charlot, S. 1993, *ApJ*, 405, 538  
 Cavaliere, A., & Vittorini, V. 2000, *ApJ*, submitted  
 Cole, S., Aragon-Salamanca, A., Frenk, C. S., Navarro, J. F., & Zepf, S. E. 1994, *MNRAS*, 271, 781  
 Driver, S. P., et al. 1998, *ApJ*, 496, 93  
 Fernandez-Soto, A., Lanzetta, K. M., & Yahil, A. 1999, *ApJ*, 513, 34  
 Fontana, A., D’Odorico, S., Poli, F., Giallongo, E., Arnouts, S., Cristiani, S., Moorwood, A., & Saracco, P. 2000, *AJ*, submitted  
 Fontana, A., Menci, N., D’Odorico, S., Giallongo, E., Poli, F., Cristiani, S., Moorwood, A., & Saracco, P. 1999, *MNRAS*, 310, L27  
 Giallongo, E., D’Odorico, S., Fontana, A., Cristiani, S., Egami, E., Hu, E., & McMahon, R. G. 1998, *AJ*, 115, 2169  
 Lilly, S. J., et al. 1998, *ApJ*, 500, 75  
 Marleau, F. R., & Simard, L. 1998, *ApJ*, 507, 585  
 Mo, H. J., Mao, S., & White, S. D. M. 1998, *MNRAS*, 295, 319  
 Odewahn, S. C., Windhorst, R. A., Driver, S. P., & Keel, W. C. 1996, *ApJ*, 472, L13  
 Poli, F., Giallongo, E., Menci, N., D’Odorico, S., & Fontana, A. 1999, *ApJ*, 527, 662 (Paper I)  
 Simard, L., et al. 1999, *ApJ*, 519, 563  
 Steidel, C. C., Adelberger, K. L., Giavalisco, M., Dickinson, M., & Pettini, M. 1999, *ApJ*, 519, 1  
 Vogt, N., et al. 1997, *ApJ*, 479, L121